

Magnetic neutron scattering study of YVO_3 : Evidence for an orbital Peierls state

C. Ulrich¹, G. Khaliullin¹, J. Sirker², M. Reehuis³, M. Ohl^{4,5},

S. Miyasaka⁶, Y. Tokura^{6,7}, and B. Keimer¹

¹*Max-Planck-Institut für Festkörperforschung, 70569 Stuttgart, Germany*

²*Theoretische Physik I, Universität Dortmund, 44221 Dortmund, Germany*

³*Institut für Physik, EKM, Universität Augsburg, 86159 Augsburg, Germany*

⁴*Institut Laue-Langevin, 156X, 38042 Grenoble, France*

⁵*Forschungszentrum Jülich GmbH, 52425 Jülich, Germany*

⁶*Department of Applied Physics, University of Tokyo, 113 Tokyo, Japan and*

⁷*Correlated Electron Research Center (CERC), National Institute of Advanced Industrial Science and Technology (AIST), Tsukuba 305-8562, Japan*

(Dated: November 14, 2018)

Neutron spectroscopy has revealed a highly unusual magnetic structure and dynamics in YVO_3 , an insulating pseudocubic perovskite that undergoes a series of temperature induced phase transitions between states with different spin and orbital ordering patterns. A good description of the neutron data is obtained by a theoretical analysis of the spin and orbital correlations of a quasi-one-dimensional model. This leads to the tentative identification of one of the phases of YVO_3 with the “orbital Peierls state”, a theoretically proposed many-body state comprised of orbital singlet bonds.

PACS numbers: 75.30.Et, 75.30.Ds, 75.50.Ee, 78.70.Nx

Materials with valence d -electrons exhibit a multitude of competing many-body states whose theoretical description is still in its infancy. Recently, much attention has focused on transition metal oxides with low-lying electronic states (termed “orbitals”) in which temperature or doping can drive phase transitions involving marked redistributions of the valence electron density (“orbital ordering”) [1]. The orbital ordering temperatures in insulating oxides (such as the widely studied manganites) are generally high and approach the temperatures at which these materials become chemically unstable. Magnetic phase transitions involving unpaired valence electrons then occur at much lower temperatures. A striking exception to this general scenario was recently discovered in insulating YVO_3 , where a series of temperature-induced magnetization reversals heralds a spontaneous redistribution of the valence electron density far below the magnetic ordering temperature [2, 3, 4].

The microscopic origin of this unusual series of phase transitions has thus far remained elusive. Given that YVO_3 is an insulator with a simple, nearly cubic lattice structure and only two localized valence electrons per vanadium atom ($3d^2$), the difficulty of obtaining a microscopic description of its phase behavior may seem surprising. It is rooted in the large number of nearly degenerate many-body states accessible to transition metal oxides with unquenched orbital degrees of freedom, a situation termed “orbital frustration”. Clearly, the orbital occupations of YVO_3 cannot be treated as temperature independent parameters and are hence affected by orbital frustration. However, while pure spin models with fixed exchange interactions have been extensively studied, quantitative solutions of models with variable spins and orbitals have thus far been obtained only in one spatial dimension (1D) [5]. In this Letter we show that

a 1D spin-orbital model contains much of the physics underlying the phase behavior of YVO_3 . The temperature induced charge density rearrangement is driven by a thermal crossover between two competing states near a zero-temperature phase transition of the model: a ferromagnet and a novel collective singlet state, the “orbital Peierls state”, that has been theoretically proposed [5] but hitherto not been observed. In this state, the superexchange energy of a system of fluctuating exchange bonds is lowered through spontaneous formation of a dimerized state with alternating strong and weak bonds, in analogy to the Peierls instability of a 1D metal.

The neutron diffraction experiments were carried out on the E5 four-circle diffractometer at the BER II reactor of the Hahn-Meitner Institute in Berlin, Germany, where Cu- or PG-monochromators selected the neutron wave vectors 7.07 \AA^{-1} and 2.66 \AA^{-1} , respectively. The data were collected with a two-dimensional position sensitive ^3He -detector. The inelastic neutron scattering experiments were carried out at the IN22 triple-axis spectrometer located at the Institut Laue-Langevin in Grenoble, France, with a pyrolytic-graphite (PG) monochromator and a PG-analyzer, both horizontally focusing. The final wave vector was fixed at either 2.66 \AA^{-1} or 4.10 \AA^{-1} . This allowed the determination of the magnon dispersion relations in an energy range up to 50 meV, with energy resolutions varying between 1 and 5 meV. The samples were untwinned single crystals of YVO_3 ($3 \times 3 \times 11 \text{ mm}$) grown by a floating zone technique described earlier [6].

The room temperature crystal structure of YVO_3 is described by the orthorhombic space group $Pbnm$ [4, 7] and lattice parameters $a = 5.2821(9) \text{ \AA}$, $b = 5.6144(8) \text{ \AA}$, and $c = 7.5283(11) \text{ \AA}$. For simplicity we will follow common practice and index the reciprocal lattice in terms of a pseudocubic subcell with (almost equal) lattice param-

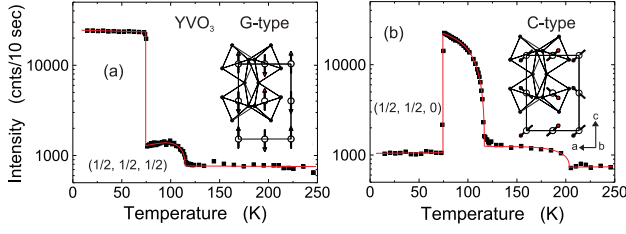


FIG. 1: Integrated intensities of (a) the $(1/2, 1/2, 1/2)$ and (b) the $(1/2, 1/2, 0)$ Bragg reflection of YVO₃ as a function of temperature. Both reflections are structurally allowed, but most of their intensity is of magnetic origin. Pictorial representations of the magnetic structures are given as insets (together with the octahedral rotation pattern corresponding to the orthorhombic cell). A structural phase transition at 200 K leads to a weak modification of the structural component of the $(1/2, 1/2, 0)$ reflection [3, 4].

eters $a/\sqrt{2}$, $b/\sqrt{2}$, and $c/2$. YVO₃ exhibits two magnetic phases. Between 1.5 K and $T_{N1} = 75$ K, we observe magnetic Bragg reflections of the type $(h/2, k/2, l/2)$ with h, k, l odd (Fig. 1a). The magnetic structure is thus of G-type, that is, antiferromagnetic in all three directions of the pseudocubic cell (inset in Fig. 1a). A full refinement of the magnetic structure ($R(F) = 0.034$) yields an ordered moment of $1.72(5)\mu_B$ oriented along c . The magnetic diffraction pattern changes at T_{N1} , and for $T_{N1} < T < T_{N2} = 116$ K reflections of the type $(h/2, k/2, l)$, with h, k odd and $l = 0$ or even, are dominant (Fig. 1b). In this temperature range, the magnetic structure is predominantly of C-type, that is, antiferromagnetic in the ab -plane and ferromagnetic along c . These observations are consistent with previous work on powder samples [7].

However, our single-crystal data now show that the high temperature phase is much more complex than previously assumed. For instance, magnetic Bragg reflections of G-type persist in this phase with diminished intensity (Fig. 1a), indicating that the spin structure is noncollinear. A refinement of the magnetic diffraction pattern ($R(F) = 0.093$) yields a G-type component of $0.30(4)\mu_B$ along c , and C-type components of $0.49(3)\mu_B$ and $0.89(2)\mu_B$ along a and b , respectively. The moments are thus canted by $\theta = 16.5(1.8)^\circ$ out of the ab plane, and the total ordered moment is $1.05(2)\mu_B$, much smaller than both the free-ion moment of $2\mu_B$ and the ordered moment of the low temperature phase at T_{N1} . The large reduction of the order parameter suggests strong quantum fluctuations in the high temperature phase.

The unusual nature of the high temperature phase is underscored by its magnetic dynamics. Representative inelastic neutron scattering data are shown in Fig. 2, and a synopsis of the magnon dispersions extracted from fits to these data is given in Fig. 3. The magnons in the low temperature phase follow a simple anisotropic Heisenberg model with exchange parameters $J_c = 5.7 \pm 0.3$ meV and

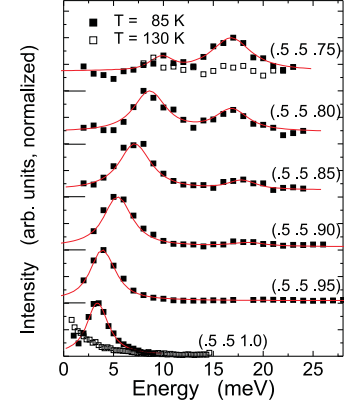


FIG. 2: Solid symbols: Inelastic neutron scattering profiles in the high temperature phase of YVO₃, showing acoustic and optical magnon branches. (Note that $l = 1$ is equivalent to $l = 0$.) The lines are the results of fits to a magnon cross section convoluted with the spectrometer resolution function [14]. Open symbols: Data taken in the paramagnetic state.

$J_{ab} = 5.7 \pm 0.3$ meV (Fig. 3a). The zone-center gaps can be attributed to a single-ion anisotropy of the form $-K_1 S_{iz}^2 + K'_1 (S_{ix}^2 - S_{iy}^2)$ with $K_1 = 0.33 \pm 0.08$ meV and $K'_1 = 0.18 \pm 0.05$ meV. Up to the first order transition at T_{N1} , the G-type magnetic correlations are weakly temperature dependent (Fig. 1a). In the high temperature phase, low energy magnons are observed at both $Q = (1/2, 1/2, 1/2)$ and $(1/2, 1/2, 0)$, as expected based on the canted spin structure (Fig. 1b). The magnon gaps at these points are identical and substantially smaller than the zone-center gap of the G-phase immediately below T_{N1} , ruling out any two-phase coexistence scenario.

The spectrum of the high temperature phase (Figs. 2 and 3b) exhibits several unexpected features. First, the magnon band width along the ferromagnetic c -axis is larger than that in the antiferromagnetic ab -plane. This violates the standard Goodenough-Kanamori rules according to which ferromagnetic superexchange interactions are generally substantially weaker than antiferromagnetic interactions. Further, the spectrum is split into optical and acoustic magnons with a gap of 5 meV between both branches. The optical/acoustic splitting, which constitutes a large fraction of the total magnon band width, can only be described by assuming two different ferromagnetic exchange bonds along the c -axis, so that the spin Hamiltonian becomes

$$H = \sum_{\langle i,j \rangle \in ab} J_{ab} (\vec{S}_i \cdot \vec{S}_j) - \sum_i K_1 S_{ix}^2 - \sum_{\langle i,j \rangle \in c} [J_c (1 \pm \delta) (\vec{S}_i \cdot \vec{S}_j) - K_2 S_{ix} S_{jx} \pm d(S_{ix} S_{jz} - S_{iz} S_{jx})] \quad (1)$$

where $S_x \parallel c$, K_1 and K_2 are the single-ion and symmetric superexchange anisotropies, and the Dzyaloshinskii-Moriya vector \vec{d} is along the octahedral tilt axis which is

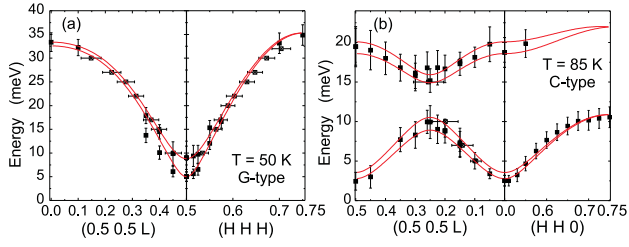


FIG. 3: Magnon dispersion relations in the (a) low and (b) high temperature magnetic phases. The lines result from diagonalizations of anisotropic Heisenberg Hamiltonians in linear spin wave theory, as discussed in the text. The effective line widths, indicated by the bars, can be attributed to the superposition of two unresolved magnon branches.

staggered along c . An excellent fit of the spectrum can be obtained by $J_{ab} = 2.6 \pm 0.2$ meV, $J_c = 3.1 \pm 0.2$ meV, $\delta = 0.35$, $K_1 = 0.90 \pm 0.1$ meV, $K_2 = 0.97 \pm 0.1$ meV, and $d = 1.15 \pm 0.1$ meV (Fig. 3b). The canting angle extracted from Eq. 1, $\theta = \frac{1}{2} \tan^{-1}[2d/(2J_c - K_1 - K_2)] = 14 \pm 1^\circ$, also agrees well with the observed value.

Because of the crystallographically indistinguishable V-V distances and bond angles along the c -axis [4], our observation of strongly alternating exchange bonds in this direction must be regarded as a signature of highly unusual orbital correlations. We now proceed to outline a quantum many-body description of these correlations and their influence on the spin dynamics; details will be published elsewhere. According to electronic structure calculations [8, 9], the vanadium t_{2g} -levels are split into a lower-lying singlet of xy -symmetry and a higher-lying doublet spanned by the xz - and yz -orbitals. A structural transition associated with a contraction of the c -axis [4] indicates that this basic hierarchy of electronic states is established around 200 K. The strong intra-atomic Hund's rule interaction stabilizes a high-spin ($S = 1$) state in which the half-occupied xy -orbital dominates the antiferromagnetic in-plane interaction at all temperatures below 200 K. Below the structural phase transition at 77 K, the degeneracy of all three t_{2g} -levels is split by lattice distortions, resulting in rigid orbital order with antiferromagnetic exchange coupling in all directions as observed experimentally.

According to a recent theory [10], however, an unusual electronic state with orbital order involving *only* the xy -orbitals is established above 77 K. In this state, the degeneracy of the xz - and yz -orbitals, which control the superexchange interaction along the c -axis, is *not* lifted by lattice distortions. Coupling to spin excitations via the superexchange Hamiltonian broadens the manifold of degenerate quantum states spanned by these orbitals into a band of overall width $J = 4t^2/U$ (where t is the V-V hopping parameter and U the intra-atomic Coulomb interaction). The band of correlated spin-orbital fluctuations is *one-dimensional*, because only c -axis bonds are

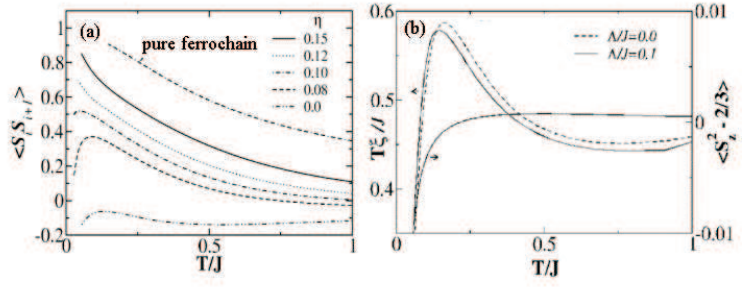


FIG. 4: (a) Nearest-neighbor pair spin correlation function $\langle \vec{S}_i \cdot \vec{S}_{i+1} \rangle$ of the 1D spin-orbital model described in the text for $\Lambda = 0$ and different values of $\eta = J_H/U$, and of a 1D ferromagnet with fixed exchange interactions, as a function of temperature. (b) Correlation length ξ (corrected for the leading $1/T$ divergence for critical excitations) for $\eta = 0.15$, and $\Lambda = 0$ and $\Lambda = 0.1J$ respectively. For the latter parameter set the spin anisotropy $\langle S_z^2 \rangle - \frac{2}{3}$ is also shown.

involved. (Spin and orbital interchain interactions are more than an order of magnitude smaller than J .) We now show that this band is unstable against dimerization, and that this “orbital Peierls” instability holds the key to the unusual magnetic properties we have observed in the C-type phase.

In addition to the overall superexchange energy scale J , the spin-orbital Hamiltonian along the c -axis contains two parameters: the Hund's rule coupling J_H (via the ratio $\eta = J_H/U$), and the spin orbit (SO) coupling Λ . To develop some intuition, we first consider the influence of the largest parameter, J , separately by setting $\eta = \Lambda = 0$. In this limit, the Hamiltonian can be written [10]

$$H = \frac{J}{2} \sum_{\langle ij \rangle} (\vec{S}_i \cdot \vec{S}_j + 1)(\vec{\tau}_i \cdot \vec{\tau}_j + \frac{1}{4}) \quad (2)$$

where $\langle ij \rangle$ denotes a nearest-neighbor pair of V-atoms along c , and $\vec{\tau}$ is a pseudospin-1/2 operator acting in the xz - and yz -orbital subspace. The energy of a single exchange bond described by this Hamiltonian is minimized by formation of an orbital singlet ($\langle \vec{\tau}_i \cdot \vec{\tau}_{i+1} \rangle = -3/4$) with an accumulation of charge between the V-atoms and ferromagnetic alignment of the spins. Hence a strong dimerization in the ground state is expected [11].

In order to elucidate the ground state properties of the full many-body Hamiltonian, we performed numerical calculations using the transfer matrix renormalization group (TMRG) method which is known to yield accurate finite-temperature correlation functions and thermodynamic properties for a variety of 1D systems [12, 13]. Some results are shown in Fig. 4. The numerically computed correlator $\langle \vec{\tau}_i \cdot \vec{\tau}_{i+1} \rangle$ extrapolates to $-3/8$ per bond at $T=0$, thus demonstrating that the ground state indeed spontaneously dimerizes into orbital singlets on every second bond as suggested by the simple consideration above (data not shown). While the exchange interaction between spins within an orbital singlet is strong and fer-

romagnetic, nearest-neighbor spins in adjacent singlets are coupled through a weak, antiferromagnetic exchange interaction; the spin pair correlator $\langle \vec{S}_i \cdot \vec{S}_{i+1} \rangle$ is therefore negative (Fig. 4a).

The spontaneous exchange bond dimerization in the ground state of the Hamiltonian Eq. 2 already hints at an explanation of the unusual magnetic spectrum observed in the high temperature phase of YVO_3 . However, a quantitative description of YVO_3 must also include the Hund's rule and SO interactions. The generalization of Eq. 2 for nonzero Hund's rule coupling is given in Refs. [10, 13], and the numerically computed correlator $\langle \vec{S}_i \cdot \vec{S}_{i+1} \rangle$ is plotted in Fig. 4a for different values of η . As expected on general grounds, the ground state for large η becomes a uniform ferromagnet with $\langle \vec{S}_i \cdot \vec{S}_{i+1} \rangle = 1$. The transition between dimerized and ferromagnetic states occurs at $\eta_c \sim 0.11$, remarkably close to the realistic value ~ 0.12 [9] for vanadium oxides.

Due to the proximity to the zero-temperature phase transition, the spin and orbital correlations at elevated temperatures exhibit an intriguing evolution. First, a pronounced maximum of the spin correlator $\langle \vec{S}_i \cdot \vec{S}_{i+1} \rangle$ as a function of temperature is apparent for the case of $\eta \lesssim \eta_c$. The origin of the initial dramatic increase upon heating lies in the weak exchange bonds between spins in adjacent orbital dimers. These bonds are highly susceptible to thermal fluctuations, and the associated increase in entropy stabilizes the orbital Peierls state. In fact, upon increasing the temperature this state quickly becomes the leading instability even for $\eta > \eta_c$, and the numerically computed dimer correlation length begins to exceed those of other possible ground states (Fig. 4b). With $J \sim J_{ab}/0.16 \sim 40$ meV extracted from the low temperature magnon dispersions following Ref. [10], the temperature range in which the dimerized phase is the leading instability coincides approximately with the high temperature phase of YVO_3 . This indicates a microscopic mechanism for the exchange bond dimerization experimentally observed in this phase. Fig. 4a also shows that the spin correlations of the spin-orbital chain are frustrated and hence weaker than those of an orbitally nondegenerate ferromagnetic chain. The suppression of the spin correlations due to orbital fluctuations provides a natural explanation for the anomalously small ordered moment observed in the high temperature phase.

Next, we address the intra-atomic SO coupling $H_{SO} = -2\lambda S_{iz}\tau_{iz}$ where $S_z \parallel c$. TMRG calculations in which this interaction is explicitly included (Fig. 4b) show that the interplay between spin-orbit and superexchange interactions gives rise to an easy-plane spin anisotropy while the entropy-driven dimerization is almost unaffected. In the temperature range of interest, the quantity $\langle S_z^2 \rangle$ drops below $\frac{2}{3}$, its value for an isotropic paramagnet. The preferred spin direction is thus the *ab*-plane, as experimentally observed in the high temperature phase of YVO_3 . These nonlocal orbital correlations are at the root

of the large superexchange anisotropies of Eq. 1. They counteract the single-ion anisotropy (which is responsible for the *c*-axis oriented moments in the low temperature phase) and account for the noncollinear spin structure in the high temperature phase. The physical origin of this effect is a compromise between the tendency of the superexchange interaction to co-align the spins and anti-align the orbital pseudospins of neighboring V-atoms, and the tendency of the SO interaction to align spin and pseudospin at every site. In analogy to a spin-flop transition (with the *c*-axis oriented orbital pseudospin playing the role of the magnetic field), a ferromagnetic alignment of *ab*-oriented spins satisfies the superexchange coupling while allowing the spins to cant out of the plane to take partial advantage of the SO coupling.

In summary, all of the unusual features of the high temperature phase of YVO_3 including the large ferromagnetic exchange coupling along the *c*-axis, the optical-acoustic splitting of the magnon spectrum, as well as the easy-plane anisotropy, the anomalously small magnitude and the large canting angle of the ordered moment are thus explained in a quasi-1D model with dynamical spin and orbital degrees of freedom. Based on this analysis a lattice dimerization is expected in the high temperature phase, but may be difficult to observe because of the large thermal and quantum fluctuations in the orbital sector and the weak lattice coupling of the t_{2g} orbitals.

-
- [1] Y. Tokura and N. Nagaosa, *Science* **288**, 462 (2000).
 - [2] Y. Ren *et al.*, *Nature* **396**, 441 (1998); *Phys. Rev. B* **62**, 6577 (2000).
 - [3] M. Noguchi *et al.*, *Phys. Rev. B* **62**, R9271 (2000).
 - [4] G.R. Blake *et al.*, *Phys. Rev. Lett.* **87**, 245501 (2001).
 - [5] Y. Yamashita, N. Shibata, and K. Ueda, *Phys. Rev. B* **58**, 9114 (1998); S.K. Pati, R.R.P. Singh, and D.I. Khomskii, *Phys. Rev. Lett.* **81**, 5406 (1998); F. Mila, B. Frischmuth, A. Deppeler, and M. Troyer, *ibid.* **82**, 3697 (1999).
 - [6] S. Miyasaka, T. Okuda, and Y. Tokura, *Phys. Rev. Lett.* **85**, 5388 (2000).
 - [7] V.G. Zubkov, G.V. Bazuev, and G.P. Shveikin, *Sov. Phys.-Solid State* **18**, 1165 (1976); H. Kawano, H. Yoshizawa, and Y. Ueda, *J. Phys. Soc. Jpn.* **63**, 2857 (1994).
 - [8] H. Sawada and K. Terakura, *Phys. Rev. B* **58**, 6831 (1998).
 - [9] T. Mizokawa and A. Fujimori, *Phys. Rev. B* **54**, 5368 (1996); T. Mizokawa, D.I. Khomskii, and G.A. Sawatzky, *ibid.* **60**, 7309 (1999).
 - [10] G. Khaliullin, P. Horsch, and A.M. Olés, *Phys. Rev. Lett.* **86**, 3879 (2001).
 - [11] S.-Q. Shen, X.C. Xie, and F.C. Zhang, *Phys. Rev. Lett.* **88**, 027201 (2002).
 - [12] For a review, see *Density-Matrix Renormalization: A New Numerical Method in Physics*, I. Peschel, X. Wang, M. Kaulke, K. Hallberg, Eds. (Springer-Verlag, New York, 1999).
 - [13] J. Sirker and G. Khaliullin, *Phys. Rev. B* **67**, 100408

(2003).

- [14] Program RESTRAX (J. Kulda, priv. comm.)